nature communications

Article

https://doi.org/10.1038/s41467-024-52753-0

Sprayable anti-adhesive hydrogel for peritoneal macrophage scavenging in post-surgical applications

Received: 6 March 2024

Accepted: 19 September 2024

Published online: 27 September 2024

Check for updates

Wonmoon Song[1,3], Changyub Lee[2,3], Haein Jeong[1], Seoyeon Kim[2] & Nathaniel S. Hwang[1,2]

Post-surgical adhesions frequently occur after intra-abdominal surgery, leading to severe complications. Despite the development of various types of adhesion barriers to address post-surgical adhesions, several limitations persist, including off-target localization, handling difficulties, and potential immunogenicity. Here, we report a spray-type adhesion barrier for broad, fast application, forming two sequential networks. The first network is formed by a polyelectrolyte complex of sulfated hyaluronic acid and chitosan, while the second network is established through pluronic® F127 thermogelation. This sprayable barrier served as both a physical protector for the damaged peritoneum and an immunomodulator for peritoneal macrophages, as evidenced its effectiveness in a rat ischemic button model. Taken together, this efficient adhesion barrier presents a promising solution for post-surgical adhesions.

Post-surgical adhesion is a type of scar resulting from peritoneal injury in intra-abdominal surgeries[1,2]. It is a common issue for the patients it affects. In the USA, more than 300,000 abdominal surgeries are performed annually[3]. Furthermore, 54 % of patients experience post-surgical adhesions following their abdominal surgeries[4]. These adhesions can lead to a range of complications, including subfertility and chronic abdominal pain, imposing significant health burdens on the patients[5–7]. However, despite its high occurence rate and associated risks, this remains unfamiliar to many surgeons. A survey among German gynecologists revealed that only 38.4 % of surgeons regularly used adhesion barriers, primarily due to the absence of cost-effective commercial products[8]. Moreover, there have been other limitations in developing adhesion barriers, such as difficulties in handling[9], inflammation[10], and inefficient delivery methods (Fig. 1)[11]. Hence, there is an unmet need for the development of effective and efficient novel adhesion barriers.

To address post-surgical adhesions, two representative strategies are known: (1) The insertion of a physical barrier between injured peritoneums[12] and (2) Anti-inflammation[4]. Physical barriers directely protect injured organs and prevent the formation of adhesion bands between organs[13]. Anti-inflammatory reagents reduce immune cell recruitment and their production of pro-inflammatory cytokines[14], thereby breaking the viscious cycle of inflammation, which impacts the severity of post-surgical adhesions[15]. In the context of these strategies, a functional hydrogel emerges as an optimal option for developing adhesion barriers[16]. Hydrogels serve as physical barriers by covering the damaged peritoneum. Furthermore, hydrogels with anti-inflammatory properties can attenuate the progression of post-surgical adhesions by synergizing with their barrier functions[17–19].

In this study, we fabricated a sprayable, anti-inflammatory adhesion barrier that improved the efficiency of adhesion barriers. The sulfated hyaluronic acid (sHA) was the main component of the sprayable adhesion barrier, serving two roles for the adhesion barrier. The first role was that the sHA could gelate in situ by blending with chitosan (Chi) through polyelectrolyte complex formation (Supplementary Fig. 1). Besides, the efficiency of this in situ gel was maximized by a dual-sprayable system. Each sHA and Chi solution was loaded into the customized dual-sprayer and sprayed individually, integrated during spraying and delivered to the target as a gel state. This system allowed for the rapid coverage of a wide area, reducing the amount of reagent

[1]Interdisciplinary Program in Bioengineering, Seoul National University, Seoul, Republic of Korea. [2]School of Chemical and Biological Engineering, Institute for Chemical Processes, Seoul National University, Seoul, Republic of Korea. [3]These authors contributed equally: Wonmoon Song, Changyub Lee.
e-mail: nshwang@snu.ac.kr

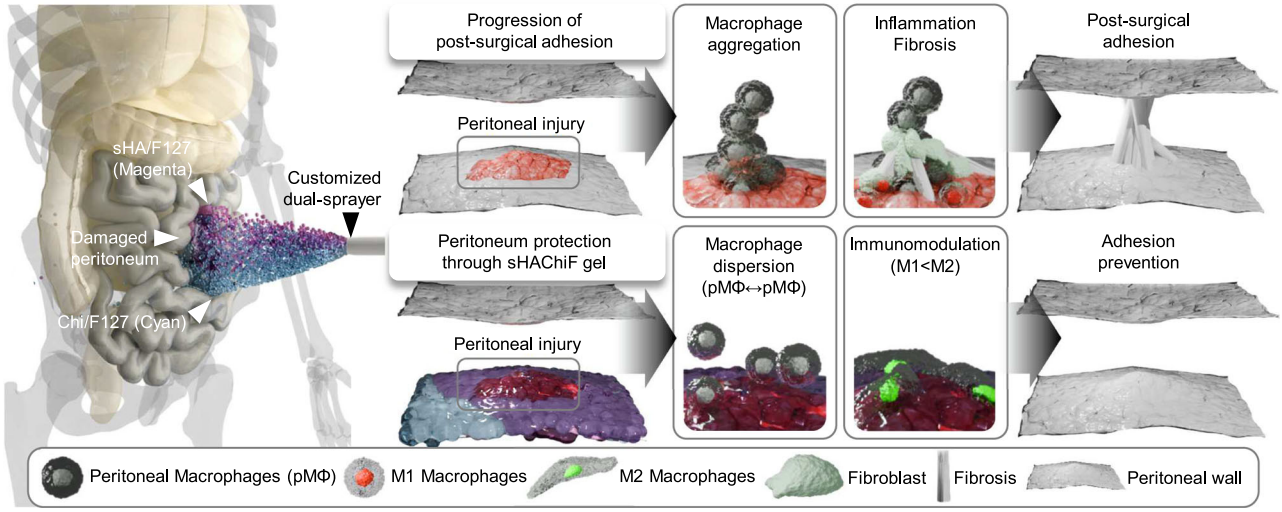

Fig. 1 | Dual-sprayable hydrogel 'sHAChiF' for the prevention of post-surgical adhesion. Using a customized dual-sprayer, two distinct components (sHA/F127 and Chi/F127) were simultaneously blended and underwent in situ gelation. The sHA in sHAChiF hydrogel acted on peritoneal injury by targeting peritoneal macrophages (pMΦs). The negative charge of sHA dispersed pMΦs, and anti-inflammatory properties of sHA polarized the pMΦs to M2 phenotype. By blocking initiation of the post-surgical adhesion through targeting pMΦs, the sHAChiF hydrogel effectively prevent post-surgical adhesion formation. Image was created using Blender 4.0.

required, improving fidelity, and saving time. However, this gelation mechanism based on polyelectrolyte complex had a disadvantage to use[20]. The gel became precipitated by the progression of electrostatic interaction between the sHA and Chi. To increase stability, we added thermoresponsive pluronic® F127 (Fig. 2a). This polymer disturbed excessive precipitate formation of the sHA/Chi complex and formed a secondary network activatable by body temperature, enhancing structural stability.

The second role of the sHA for the anti-adhesion barrier was immunomodulation that targeting peritoneal macrophages. It is well-documented that sHA can modulate activity of macrophage by blocking NF-κB signaling and its downstream expression of pro-inflammatory cytokines[21,22]. This accelerates M2 polarization of the peritoneal macrophages and attenuates pro-inflammatory cytokines. Additionally, it has been discovered that the anionic polymer could disrupt the aggregation of peritoneal macrophages by blocking their scavenging receptors[23]. As expected, sHA also could disperse the peritoneal macrophages. Harnessing these multifunctional effects of the sHA, the sHA/Chi/F127 sprayable gel, which we called sHAChiF, we demonstrated its therapeutic effect by using a rat ischemic button model. The sHAChiF was delivered to the ischemic buttons rapidly via the customized dual-sprayer, and showed better protection against post-surgical adhesion than the commercial patch-type adhesion barrier Seprafilm®.

Results

Fabrication of sHAChiF hydrogel

To develop the sHAChiF, sHA was prepared through the sulfation of HA. The degree of sulfation (DS) of the hydroxyl groups in the sHA was determined via elemental analysis, and the molecular weight of sHA was measured using gel permeation chromatography (GPC) (Supplementary Table 1). The DS of sHA was 62.63 ± 4.28%, with an average molecular weight of 82.88 ± 5.98 kDa. Another component of the sHAChiF, Chi, was dissolved in hydrochloric acid to reduce its viscosity. It is known that the size of the anions in a Chi solution can affect its viscosity[24]. Among the acids used to prepare the Chi solution, chloride ions were found to be optimal for reducing the viscosity of the Chi due to their smaller size compared to other polyions, such as acetic acid or lactic acid[25].

sHA exhibits attractive characteristics as a functional biomaterial. It has been demonstrated that sHA effectively possesses immunomodulatory functions, thereby supporting wound regeneration and alleviating dermatitis[22]. Furthermore, sHA exhibits resistance against hyaluronidase and degrades slowly, effectively addressing the issue of rapid degradation associated with HA[26]. In order to harness these appealing characteristics, we employed a strategy to utilize sHA by creating a hydrogel: Polyelectrolyte complex formation via electrostatic interaction with a cationic polymer. Hence, we chose the well-known biocompatible cationic glycosaminoglycan, Chi, to enable the transformation of sHA into a hydrogel. When sHA was combined with Chi, the sHA/Chi complex underwent gelation (Supplementary Fig. 1a). This sHA/Chi gel could be injected through a syringe needle, whereas the HA/Chi complex failed to gel due to precipitation (Supplementary Fig. 1b). Notably, not only was injection possible, but the sHA/Chi complex also readily gelated when sprayed onto its target (Supplementary Fig. 1c). This highlights the potential of the sHA/Chi complex as an in situ hydrogel. However, it should be noted that the sHA/Chi complex did not achieve a stable, evenly distributed network structure. Following complexation, precipitation of the sHA/Chi complex occurred, similar to the behavior observed with the HA/Chi complex (Supplementary Fig. 1a). This phenomenon stemmed from excessive electrostatic interactions between sHA and Chi, necessitating the introduction of pluronic® F127 as a secondary network to mitigate this polyelectrolyte complex formation.

The sHA/Chi/F127 mixture rapidly developed an opaque gel structure upon mixing at 25 °C (Fig. 2b). To optimize the gelation conditions of the sHA/Chi/F127 mixture, we conducted a screening of various formulations using the inverted vial test (Fig. 2c, d). The symbols in Fig. 2c, d denote the outcomes of the test. Specifically, the circle indicates successful gelation, whereas the triangle represents gelation failure. It was observed that when the pluronic® F127 concentration was set at 19%, nearly all formulations failed to undergo gelation (Fig. 2c). Conversely, when the pluronic® F127 concentration was set at 20%, a Chi-dependent gelation behavior was observed (Fig. 2d). Higher Chi concentrations facilitated gelation of the sHA/Chi/F127 complex. In contrast, higher sHA concentrations led to gelation failure by precipitation of the complex. Based on the screening results, we optimized the formulation conditions to consist of sHA (1.0%), Chi (1.0%),

https://doi.org/10.1038/s41467-024-52753-0

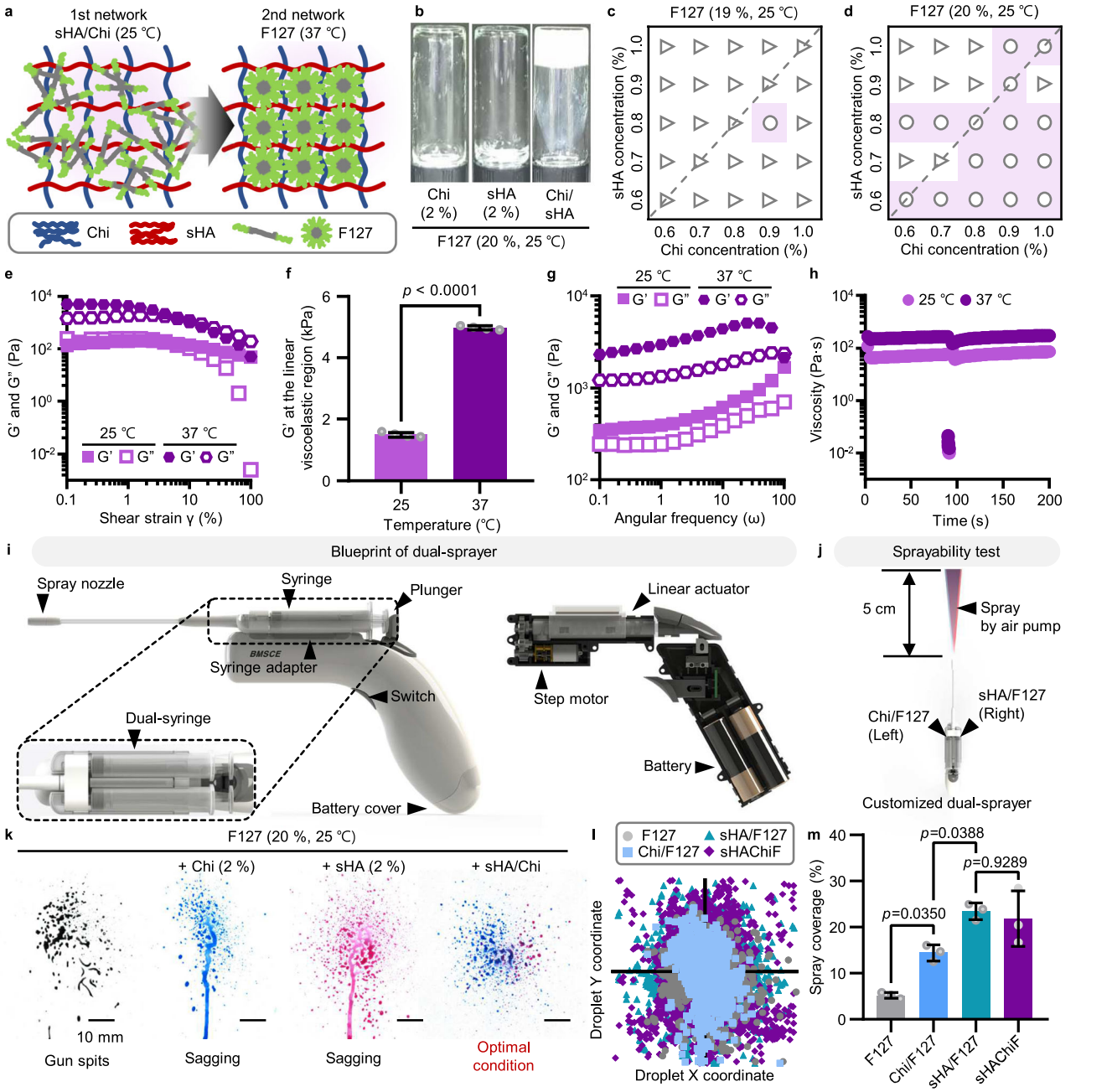

Fig. 2 | Mechanical characterization of sHAChiF. a Schematic illustration of the crosslinking mechanism of sHAChiF. **b** Representative images of inverted vial test of sHAChiF at 25 °C. Screening of optimal gelation condition with various concentration of components of sHAChiF. Screening plot with pluronic® F127 19% (**c**), and pluronic® F127 20% (**d**). Rheological properties of sHAChiF. Oscillatory strain sweeps of sHAChiF performed at 5 rads^{-1} (**e**), quantification of storage modulus (G') of sHAChiF at the linear viscoelastic region during oscillatory strain sweeps (**f**), Oscillatory frequency sweeps of dual-sprayable hydrogels performed at 5% strain (**g**), and three-interval-thixotropy test of dual-sprayable hydrogels performed at 100% strain (**h**). **i** 3D rendering design of the customized dual-sprayer for 3D printing (left), 3D rendering design of the components for the customized dual-sprayer (right). **j** Schematic illustration of sprayability test of sHAChiF with customized dual sprayer. Representative images of spray formation of sHAChiF (**k**), overlayed droplet distributions of sprayed sHAChiF (**l**), quantification of spray coverage of sHAChiF (**m**). Data are shown as mean ± SD ($n = 4$ independent samples in **e**–**h**; $n = 3$ independent samples in **k**–**m**). Two-tailed unpaired t-test was used for statistical analysis of **f**. One-way ANOVA with Tukey post-hoc test was used for statistical analysis of **m**. Source data are provided as a Source Data file. Image was created using Solidworks 2021.

and pluronic® F127 (20%). This optimized gel formulation was referred to as sHAChiF.

Interestingly, it should be noted that this complex remained unstable at 25 °C, leading to slow precipitation, particularly when the concentration of pluronic® F127 was 19% (Supplementary Fig. 2a). Although the precipitation behavior was less pronounced, the pluronic® F127 (20%) condition did not entirely prevent sHAChiF gel from precipitating (Supplementary Fig. 2b). This precipitation resulted in the formation of clear gel (Supplementary Fig. 2c). However, sHAChiF exhibited stable networks and maintained its state at 37 °C. Thus, the presence of a secondary network formed by pluronic® F127 at body temperature (37 °C) played a crucial role in stabilizing the polyelectrolyte complex. Furthermore, it is imperative to keep the two components, sHA, and Chi, separated until use.

Mechanical characterization of sHAChiF hydrogel

To investigate the mechanical characteristics, we conducted rheological tests to assess the viscoelasticity of the sHAChiF. The amplitude sweep test revealed two distinct behaviors within a strain range from 0.1 to 100% (Fig. 2e). The storage modulus G' of the linear viscoelastic region of the sHAChiF at 37 °C was measured at 5.0 ± 0.1 kPa, significantly higher than the G' at 25 °C, which was 1.5 ± 0.8 kPa (Fig. 2f). This demonstrated that the thermosensitive gelation of Pluronic® F127 significantly enhanced the mechanical strength of the sHAChiF, increasing it 3.3-fold higher. This trend was consistently observed in the frequency sweep test across the angular frequency range from 0.1 to 100 rad s^{-1} (Fig. 2g). At 25 °C, the G' and the G'' values were close to each other, indicating a viscous semi-gel state similar to petroleum jelly[27]. At 37 °C, the G' value exceeded the G'' value, indicating that the sHAChiF maintained its gel-like state. The temperature-sweep test revealed that the concise thermogelation temperature of sHAChiF was 30.05 °C (Supplementary Fig. 3a). Given that the exposed surface body temperature can easily dropp during laparatomy[28], this thermogelation temperature, being below 37 °C, would be advantageous for stable gelation. We also identified whether the mechanical enhancement of sHAChiF was a resulted of thermogelation. The inverted vial test of sHAChiF, conducted as the temperature dropped from 37 °C to 4 °C demonstrated that the network could be controlled by temperature (Supplementary Fig. 3b). Interestingly, the sHAChiF gel was not completely liquid at 4 °C. This was attributed to the first network, which was formed by the polyelectrolyte complex between sHA and Chi.

To investigate the gel-like state of sHAChiF further, a three-interval-thixotropy test was conducted (Fig. 2h). At 25 °C and 37 °C, the viscosity of the sHAChiF recovered immediately after a 100% strain application. This rapid self-healing property is attributed to the reversible networks within the sHAChiF. After mechanical stress, the disrupted networks of the sHAChiF easily reformed through network reconnection. These unique properties render the sHAChiF particularly advantageous for reliable adhesion to the peritoneum compared to other patch-type adhesion barriers. For instance, Seprafilm® is prone to tearing during application, impeding its handling and coverage of damaged peritoneal areas[29].

Optimization of sHAChiF for sprayable system

The delivery of biomaterials through spraying offers significant advantages as it enables wide and rapid distribution[30,31]. This delivery method is particularly crucial for adhesion barriers due to the primary limitations associated with conventional adhesion barriers, such as cost-effectiveness[32], handling difficulty[33], and localization failure[34]. To address these issues, it is essential to achieve adequate coverage of peritoneal wounds with a minimal amount of material and stabilize on the target. Building upon the previously mentioned results, which indicated that the sHAChiF tended to precipitate when incubated at room temperature for an extended period, we designed a dual-sprayer system to facilitate in situ blending and in situ gelation of the sHAChiF (Fig. 2i). By pressing the switch of the dual-sprayer, torque generated by step motor was converted into linear movement by linear actuator. This force transfer enabled the plunger to be pushed, effectively expelling the liquid loaded into the syringe through a process where it was injected and then sprayed using compressed air (Supplementary Movie 1). Each solution of sHA/F127 and Chi/F127 could be separately loaded into syringes and assembled together using a syringe adaptor. Through the customized dual-sprayer, sHA/F127 and Chi/F127 were sprayed simulatneously, forming sHAChiF immediately.

To make the Chi/F127 solution suitable for spraying, careful consideration was given to the choice of acid for dissolving Chi. When Chi was dissolved in an acetic acid solution, the Chi/F127 solution exhibited high viscosity, making it challenging to spray (Supplementary Fig. 4a). However, by changing the type of acid from acetic acid to hydrochloric acid, the spray behavior of the Chi/F127 solution was improved, resulting in a 4.8-fold increase in the spray area (Supplementary Fig. 4b). Consequently, hydrochloric acid was selected as the solvent for dissolving the Chi/F127 solutions. Viscosity measurements were performed at a shear stress of 1000 s^{-1} to simulate the shear stress experienced during spraying (Supplementary Fig. 4c). While the viscosity of the Chi/F127 solution increased with higher Chi concentration, this behavior did not negatively impact its sprayability (Supplementary Fig. 4d).

We subsequently validated the sprayability of the sHAChiF using the customized dual-sprayer, which allowed two different materials to be loaded into each syringe and sprayed simultaneously (Fig. 2j). In this setup, we sprayed the Chi/F127 solution and sHA/F127 solution. The nozzle diameter was 1 mm, the flow rate was 10 mL min^{-1}, the air pressure was 100 kPa, and the test distance from the spray nozzle was 5 cm (Supplementary Table 3). To aid in visualization, color dyes were added to each sHAChiF component (Pluronic® F127: Black, Chi/F127: Blue, and sHA/F127: Red).

Notably, the pluronic® solution (20 %) alone at 25 °C exhibited high viscosity and failed to be sprayed evenly, resulting in a gun-spit pattern (Fig. 2k). In contrast, Pluronic® F127 solutions containing either Chi (2%) or sHA (2%) showed lower viscosity and sagged after being sprayed onto the target surface. This behavior of concentration-dependent gelation in Pluronic® F127-polysaccharide mixtures has been previously documented[17]. A low content of polysaccharide can hinder the gelation of Pluronic® F127 micelles, while a high content of polysaccharide, which can form its own networks, assists in Pluronic® F127 gelation[18]. However, the sHAChiF exhibited a clear, broad spray pattern due to the synergistic gelation resulting from the rapid formation of polyelectrolytes and Pluronic® F127 micelles.

The spray patterns of these solutions were compared by overlapping all patterns (Fig. 2l). The values for spray coverage for Pluronic® F127 alone, Chi/F127, sHA/F127, and sHAChiF were determined to be 5.18 ± 0.64%, 14.4 ± 1.76%, 23.5 ± 1.80%, and 21.9 ± 6.01%, respectively (Fig. 2m). These trends were consistent with the observed spray pattern images. Notably, the Chi/F127 group exhibited lower spray coverage than the sHA/F127 and sHAChiF groups, primarily due to the higher viscosity of the Chi/F127 solution compared to the other groups.

To test the sprayability of sHAChiF under realistic conditions, we set up a heating pad-attatched whiteboard and heated the surface to 37 °C. Then, we sprayed the sHAChiF onto the whiteboard (Supplementary Movie 2). A black dye was added to each sHAChiF solution for contrast. A small amount of sHAChiF flowed down right after spraying. However, within 5 s, the sHAChiF stopped flowing and remained in place. This optimized condition, where sHAChiF was sprayable and rapidly gelated within 5 s, was deemed suitable for use as a sprayable biomaterial.

In vitro biocompatibility and immunomodulation of sHAChiF hydrogel

Biocompatibility plays a pivotal role in determining the suitability of materials for use within the human body. Materials lacking biocompatibility can exacerbate immune responses in peritoneal wounds following laparotomy, potentially leading to severe post-surgical adhesions. In this context, we conducted in vitro assessments to establish the safety of sHAChiF. Initially, we exposed NIH-3T3 fibroblasts to sHAChiF and its constituent components, sHA and Chi (Fig. 3a). All groups exhibited no toxicity towards NIH-3T3 fibroblasts (Fig. 3b).

Furthermore, sHA has previously been recognized for its ability to inhibit NF-κB signaling in macrophages and reduce the release of pro-inflammatory cytokines during inflammation[22]. This anti-inflammatory property is of paramount importance in functional hydrogels designed as adhesion barriers. To investigate whether sHA within the sHAChiF could also serve as an anti-inflammatory component, we subjected the

https://doi.org/10.1038/s41467-024-52753-0

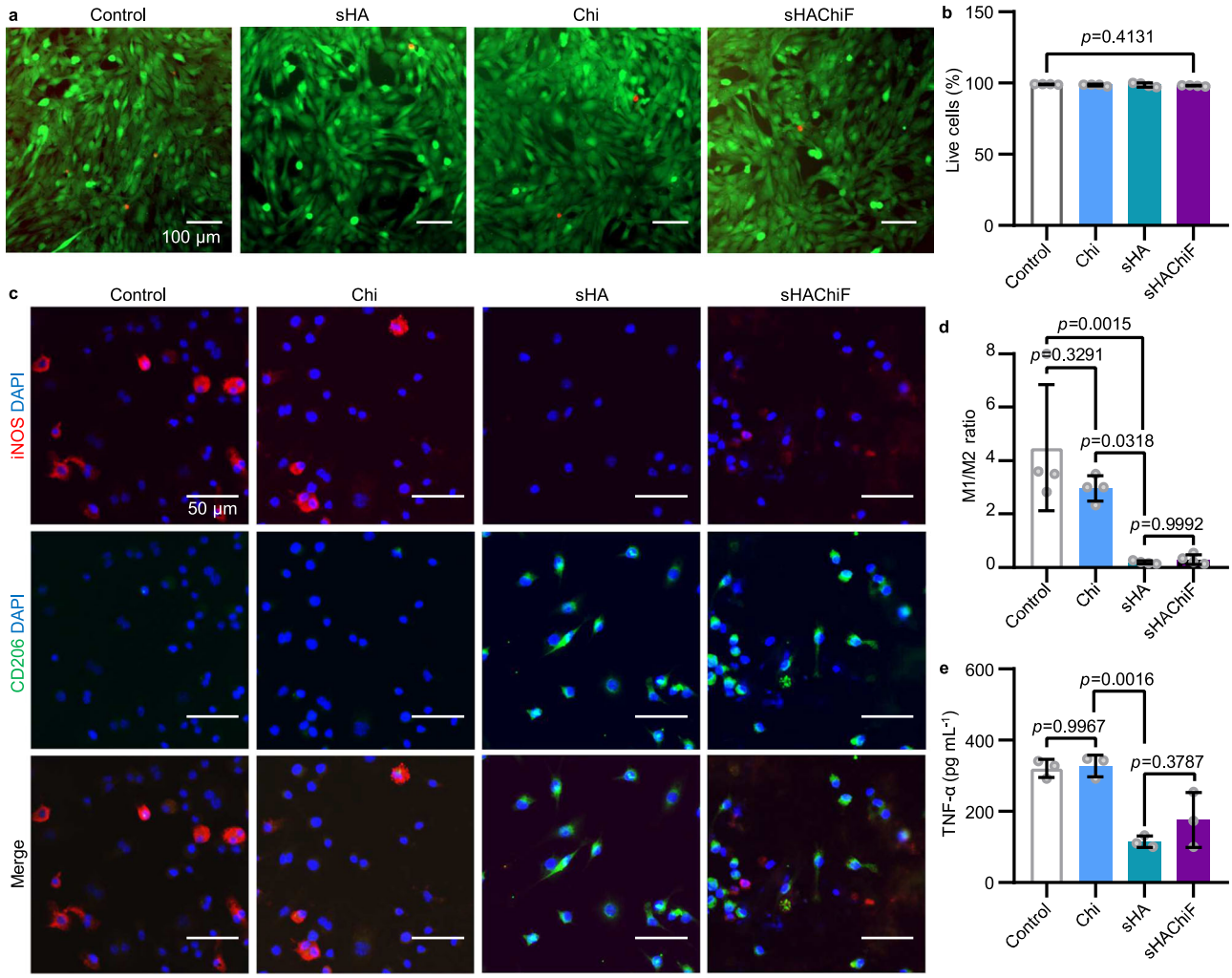

Fig. 3 | In vitro biocompatibility and in vitro immunomodulation of sHAChiF. **a** Representative Live&Dead assay fluorescence images of NIH-3T3 cells incubated with sHAChiF of different compositions (Scale bar = 100 μm). **b** Quantification of the live NIH-3T3 cells by Live&Dead assay. **c** Representative iNOS and Arg1 immunofluorescence staining of LPS-treated RAW264.7 macrophages incubated with sHAChiF (Scale bar = 50 μm). **d** Quantification of the M1/M2 ratio of RAW264.7 macrophages. **e** Quantification of TNF-α secreted by LPS-treated RAW264.7 macrophages. Data are shown as mean ± SD ($n = 4$) independent samples in **a**,**b**; $n = 4$ independent samples in **c**,**d**; $n = 3$ independent samples in **e**. One-way ANOVA with Tukey post-hoc test was used for statistical analysis of **b**,**d**,**e**. Source data are provided as a Source Data file.

sHAChiF to the RAW264.7 mouse macrophage cell line for 24 h, followed by cell activation using lipopolysaccharide (LPS) for an additional 24 h.

Using immunocytochemistry with iNOS as an M1 macrophage marker and CD206 as an M2 macrophage marker, we observed that the sHAChiF effectively protected RAW264.7 cells from LPS-induced stimulation (Fig. 3c). Intriguingly, the sHAChiF exhibited significant immunomodulatory effects on RAW264.7 cells, even in the presence of an inflammatory stimulus from LPS. In sHAChiF-treated RAW264.7 cells, CD206 expression predominated, with only a few cells expressing iNOS, resembling the sHA-treated groups. Furthermore, RAW264.7 cells in the sHAChiF and sHA groups displayed a morphological shift towards the M2 phenotype, characterized by an elongated and stretched appearance. In contrast, control and Chi-treated RAW264.7 cells exhibited high iNOS expression and low CD206 expression, indicating an M1 macrophage state, with spherical morphology being a typical feature. The M1/M2 ratio revealed those trends (Fig. 3d). The M1/M2 ratio of control and Chi-treated RAW264.7 cells was measured at 4.48 ± 2.40 and 2.96 ± 0.48, respectively, indicating their M1-like state. In contrast, the M1/M2 ratio of sHA and sHAChiF-treated RAW264.7 cells was determined to be 0.20 ± 0.06 and 0.30 ± 0.18, signifying their M2-like state.

To investigate the ability of sHA and sHAChiF to regulate inflammation, we quantified the expression of TNF-α, a representative pro-inflammatory cytokine, in LPS-treated RAW264.7 cells. The results were compelling, with both sHA and sHAChiF-treated groups showing a significant reduction in TNF-α expression (Fig. 3e). The control and Chi groups exhibited TNF-α levels of 320.04 ± 25.55 $pgmL^{-1}$ and 327.42 ± 30.56 $pgmL^{-1}$, respectively, whereas the sHA and sHAChiF groups achieved 113.76 ± 16.11 $pgmL^{-1}$ and 175.38 ± 77.14 $pgmL^{-1}$ respectively, representing a remarkable 1.8- to 2.8-fold reduction in TNF-α levels. This underscores the safety and, importantly, the anti-inflammatory efficacy of sHAChiF at the in vitro level.

In vivo biocompatibility and stability of sHAChiF hydrogel

To assess in vivo biocompatibility of the sHAChiF, a luminol assay was conducted. Luminol serves as a sensitive inflammation detector activated by myeloperoxidase produced by neutrophils or monocytes[35]. Six different materials (1: PBS, 2: Latex bead, 3: pluronic® F127, 4: Chi/F127, 5: sHA/F127, and 6: sHAChiF) were subcutaneously implanted into the dorsal area of C57BL/6 mice (Fig. 4a). After 4 d, the activated

https://doi.org/10.1038/s41467-024-52753-0

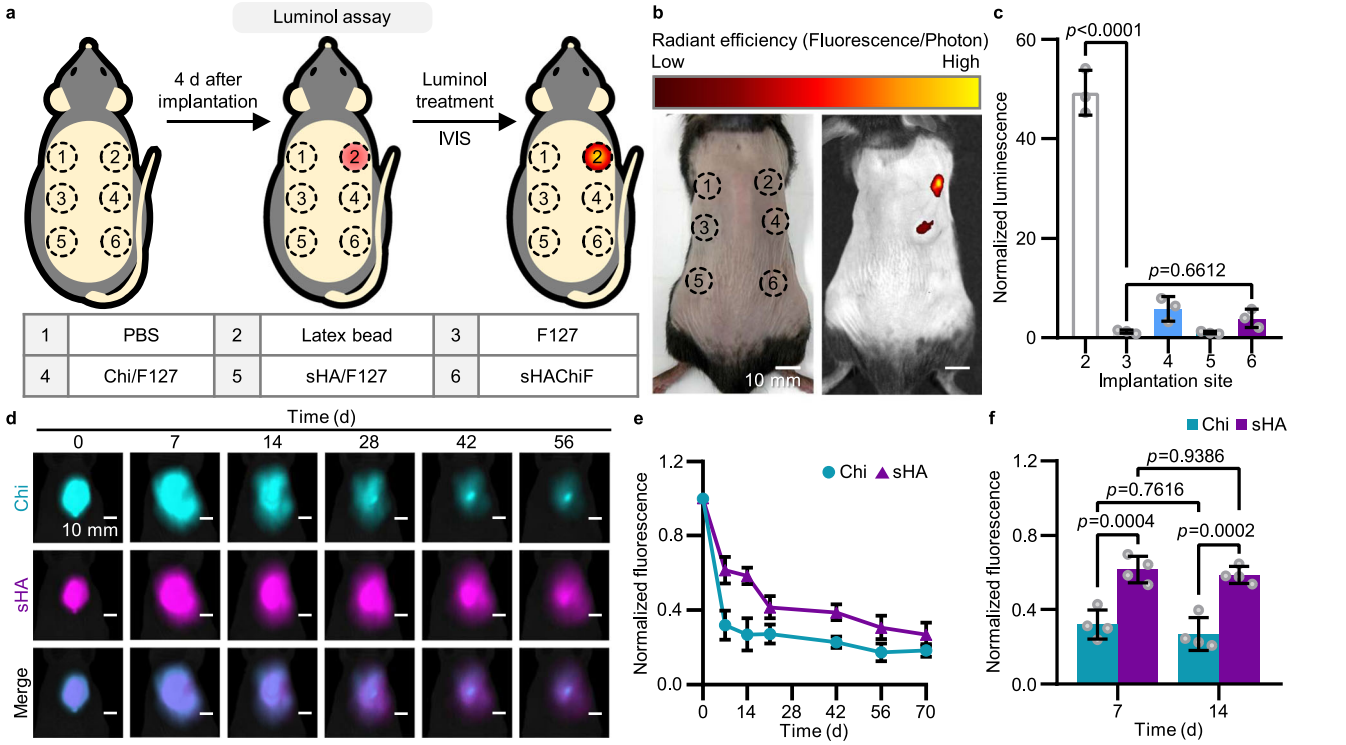

Fig. 4 | In vivo biocompatibility and in vivo retention behaviors of sHAChiF. **a** Schematic illustration of the in vivo biocompatibility imaging of sHAChiF with various formulations by luminol assay. **b** Representative IVIS images of bright field (left) and bioluminescence (right) of luminol activity for implanted sHAChiF in C57BL/6 mice (Scale bar = 10 mm). **c** Quantification of bioluminescence efficiencies of luminol activities for implanted sHAChiF in the mice. **d** Representative IVIS images of fluorescence by Cy5.5-conjugated Chi ($Chi^{Cy5.5}$; cyan; pseudocolor), and Cy7.5-conjugated sHA ($sHA^{Cy7.5}$; magenta; pseudocolor) in sHAChiF at various time points (Scale bar = 10 mm). **e** In vivo retention profiles of $Chi^{Cy5.5}$ and $sHA^{Cy7.5}$ in sHAChiF over time through calculation of fluorescence intensity, normalized by fluorescence at 0 d. **f** Quantification of normalized sHAChiF in vivo retention at 7 d and 14 d. Data are shown as mean ± SD (n = 3) independent samples in **b**,**c**; $n = 4$ independent samples in **d**–**f**. One-way ANOVA with Tukey post-hoc test was used for statistical analysis of **c**,**f**. Source data are provided as a Source Data file. Image was created using PowerPoint.

luminol at the inflammation site was detected using IVIS (Fig. 4b). PBS and latex beads were used as negative and positive controls, respectively. Luminescence levels were normalized against the basal signal of normal skin. The luminescence at the latex bead site exhibited the highest intensity, showing 49.27 ± 4.46, which represented 49-fold higher inflammation level than normal tissue (Fig. 4c). Compared by this positive control, other groups showed negligibly lower signals.

Adhesion barriers should maintain their structure for a minimum of 7 to 14 d[36]. If degradation occurs too rapidly, the adhesion barrier may lose its ability to seal the damaged peritoneum, potentially leading to post-surgical adhesions despite the use of an adhesion barrier. To determine the in vivo retention time of sHAChiF, we subcutaneously implanted sHA/F127, Chi/F127, and sHAChiF in Balb/c-nu mice to compare the degradation kinetics among them (Fig. 4d). We labeled the components with NIR dyes, with Chi conjugated with Cyanine 5.5 ($Chi^{Cy5.5}$, Excitation 684 nm, Emission 710 nm), and sHA with Cyanine 7.5 ($sHA^{Cy\ 7.5}$, Excitation 788 nm, Emission 808 nm). By imaging and measuring the fluorescence of Cy5.5 from $Chi^{Cy5.5}$ and Cy7.5 from $sHA^{Cy7.5}$, we could track the residual amount of sHAChiF.

The in vivo retention profile in mice was recorded over a span of 70 d. Both Chi and sHA within sHAChiF demonstrated rapid elimination up to the 14 d, followed by a slower removal trend (Fig. 4e). Specifically, 85.95 ± 3.33% of Chi and 76.21 ± 3.93% of sHA fluorescence in sHAChiF had been cleared by the end of the 70 d period. This degradation pattern of sHAChiF could be attributed to the collapse of the network and diffusion mechanisms. In the Fig. 4d, the diffusion behavior of sHAChiF was observed. As the primary network of sHAChiF relied on electrostatic potential, which was reversible, Chi and sHA could be released from the implantation site. To assess whether the retention of sHAChiF was suitable as an adhesion barrier, we quantified the remaining fluorescence of sHA and Chi in sHAChiF at 7 d and 14 d after implantation (Fig. 4f). After 7 d of implantation, 35.67 ± 5.30% of Chi and 58.92 ± 9.35% of sHA in sHAChiF remained in the body. At 14 d, 25.49 ± 3.33% of Chi and 54.26 ± 5.51% of sHA in sHAChiF were still present. That is, the half-life of sHA in subcutaneous implantation was close to 14 d. This retention profile demonstrated the potential of sHAChiF as an adhesion barrier that could persist during the post-surgical adhesion progression period.

This retention behavior also could be considered that sHAChiF operated as a hydrogel, releasing sHA in a sustained manner. The controlled release of sHA from sHAChiF had the potential for serving as an effective, long-term anti-inflammatory hydrogel[22]. It was worth noting that one potential limitation was the possibility of prolonged inflammation during wound healing, which could pose risks in the event of infection[5]. On the other hand, the advantageous feature of functional hydrogels capable of loading bioactive drugs for a synergistic therapeutic effect would allow for the potential complementation of sHAChiF's anti-inflammatory function by incorporating antimicrobial drugs.

Scattering of peritoneal macrophages induced by sHAChiF hydrogel through interaction with sHA

Disrupting peritoneal macrophages has been demonstrated as an effective therapeutic strategy. Zindel et al. revealed that $GATA6^+$ peritoneal macrophages, often referred to as large peritoneal macrophages (LPM), aggregate in response to peritoneal injuries, initiating post-surgical adhesion[23]. This aggregation was mediated by the recognition of damage-associated molecular patterns (DAMPs) by

scavenger receptors on LPM and could be inhibited by anionic polymers that bound to these scavenger receptors. Given this behavior of LPM, we hypothesized that the strong negative charge of sulfated hyaluronic acid (sHA) might have a similar effect.

To investigate this, we initially assessed the ability of sHA to disperse peritoneal macrophages. The DS of sHA was detailed as DS 1 (25–50%), DS 2 (50–75%), and DS 3 (75–100%) to determine whether the anionic charge of sHA could influence the behavior of peritoneal macrophages. Peritoneal macrophages tend to aggregate in a calcium-dependent manner and can be dissociated by EDTA[23]. Interestingly, the addition of chitosan to peritoneal macrophages promoted aggregation, but peritoneal macrophage aggregates did not form in the sHA-treated groups (Fig. 5a). Moreover, this effect seemed to increase with the degree of sulfation of sHA, indicating that anionic sHA can scatter peritoneal macrophages (Fig. 5b).

To verify if this phenomenon could be observed in vivo, we conducted experiments using $Chi^{Cy5.5}$ and $sHA^{Cy7.5}$ to visualize the actions of sHAChiF in peritoneal wounds. In a hepatic thermal injury model[37], we created a small perforation in the peritoneal wall and induced thermal injury to the liver using a heated rod (Fig. 5c). Subsequently, we treated the liver injury site with NIR dye-conjugated sHAChiF, while simultaneously staining peritoneal macrophages with APC/Fire™ 750 anti-F4/80 antibody. This approach enabled us to visualize peritoneal macrophages within the liver injury area using IVIS.

The results revealed that sHA and sHAChiF exhibited significantly different behaviors in response to peritoneal injury compared to Chi (Fig. 5d). Peritoneal macrophages were rapidly recruited to the damaged liver area, showing a 1.4-fold increase in fluorescence compared to normal tissues (Fig. 5e). When Chi was applied to the wound, it did not offer protection to the liver injury, as there was no significant difference in fluorescence between the control and Chi-treated groups. However, the Cy5.5 fluorescence signal in the liver wound was 3.4-fold higher than in normal tissues, indicating that Chi could be recruited to the wound (Fig. 5f). This phenomenon appeared to be due to the electrostatic interaction between cationic Chi and anionic cell surfaces. In contrast, Chi within sHAChiF exhibited even higher fluorescence, recording a 5.9-fold increase compared to normal tissues. This could be attributed to the retention of sHAChiF at the application site (liver wound).

In contrast, sHA effectively dispersed peritoneal macrophages, with no difference in fluorescence between the liver wound and other tissues. Surprisingly, sHA also demonstrated strong targeting behavior toward the wound, displaying a 15.2-fold increase in fluorescence compared to normal tissues (Fig. 5f). The fluorescence of sHA in sHAChiF was 28.3-fold higher than normal tissues. This could also be a similar result of Chi, showing the retention of sHAChiF. To determine if this behavior was attributed to the negative charge, we performed the same experiment using smaller molecules, indocyanine green (ICG) and methylene blue (MB) (Supplementary Fig. 5a). The ICG and MB produced results similar to sHA and Chi, respectively (Supplementary Fig. 5b). ICG showed a 12.5-fold increase in fluorescence in the liver injury (Supplementary Fig. 5c), while MB exhibited a 1.7-fold increase (Supplementary Fig. 5d). This suggested that the scavenging activity of peritoneal macrophages might be responsible for these outcomes. Furthermore, sHAChiF on the wound effectively prevented peritoneal macrophages from accumulating, while sHA and Chi maintained their fluorescence in the treated area.

To investigate whether peritoneal macrophages exclusively took up sHA, we conducted flow cytometry on mouse peritoneal lavage fluid after treatment with $sHA^{Cy7.5}$ (Fig. 5g). CD11b and F4/80 was selected to distinguish between LPM ($CD11b^{+}$, $F4/80^{High}$) and Small peritoneal macrophage (SPM, $CD11b^{+}$, $F4/80^{Low}$) populations (Supplementary Fig. 6a). Initially, we determined whether LPM predominantly took up sHA, potentially through the scavenger receptor, as previously reported[23]. Peritoneal cells were initially gated to identify sHA^{+} populations (Fig. 5h). Subsequently, we analyzed the distribution of LPM and SPM within the sHA^{+} groups (Fig. 5i). Surprisingly, our findings indicated that 86.35 ± 4.89% of the peritoneal cells that took up sHA were LPM, while only 3.28 ± 1.72 % were SPM (Fig. 5j). Additionally, in the sHA^{-} population, LPM and SPM percentages were 1.90 ± 0.67%, and 1.26 ± 0.47 %, respectively. This dramatic difference in uptake clearly demonstrated the selective binding of sHA to LPM populations. To further confirm this trend, we analyzed how many LPMs and SPMs actually took up the sHA (Supplementary Fig. 6b). Interestingly, 95.58 ± 1.45% of LPMs took up sHA, while, only 34.70 ± 6.50% of SPMs did so (Supplementary Fig. 6c). Collectively, we provided evidence that nearly all LPMs were influenced by anionic sHA. This observation suggested that sHA might selectively interact with LPMs.

Prevention of rat post-surgical adhesion by treating the dual-sprayable hydrogel

Adhesion barrier blocks post-surgical adhesion by physically isolating the peritoneal wound from other organs[15]. We generated 8 ischemic buttons on the abdominal wall of the Spraque-Dawley rat (SD rat) and the sHAChiF spray could be spread widely to the damaged peritoneal wall and rapidely gelated right after spraying (Fig. 6a and Supplementary Movie 3). The barrier effect of the sHAChiF was compared with Seprafilm® as a benchmark product. 7 d after surgery, severe peritoneal adhesion occurred at control and Seprafilm® groups, forming dense adhesion band on the ischemic buttons. In the contrary, sHAChiF maintaned its coverage on the ischemic buttons and protected them from post-surgical adhesion (Fig. 6b). This tendency was also observed by Masson's trichrome staining data. Collagens were deposited between the ischemic buttons and other organs (Fig. 6c).

The severity of the adhesion formation was scored according to specific criteria, raing 0 ~ 5 (Fig. 6d). The percentage of the occurrence of the post-surgical adhesion on each ischemic button was measured (Fig. 6e). Control group with PBS treatment after surgery showed the most frequent adhesion formation as 80.00 ± 11.20%. Seprafilm® were recorded as 70.00 ± 20.92%, which couldn't block the occurence of post-surgical adhesion efficiently. sHAChiF significantly lowered the adhesion formation to 20.00 ± 20.92%. The stable barrier formation ability of the sHAChiF would protect the post-surgical adhesion formation well. Also, the severity of the adhesion was dramatically lowered at the sHAChiF treated group, compared with control and Seprafilm® groups, which was almost zero score (Fig. 6f).

To assess the stability of sHAChiF in a rat post-surgical adhesion model, we conducted measurements of the retention profiles of Chi and sHA within sHAChiF using fluorescence imaging with $Chi^{Cy5.5}$ and $sHA^{Cy7.5}$ by IVIS, employing the same methodology as depicted in (Fig. 6g). Similar to the results observed in the mouse subcutaneous implantation model, sHAChiF in the rat ischemic button model exhibited a prolonged retention period exceeding 14 d. The fluorescence of Chi and sHA in sHAChiF at 7 d after surgery were recorded at 70.93 ± 7.30% and 78.54 ± 11.85%, respectively. Moreover, at 14 d, 39.14 ± 7.36% of Chi and 49.96 ± 4.42% of sHA remained detectable. These findings demonstrate that sHAChiF within the peritoneum retained its integrity for more than 14 d, establishing its stability as an effective adhesion barrier. The interaction network between Chi and sHA gradually collapsed over time, resulting in a slow removal process. At 56 d, a substantial portion had been eliminated, with 88.81 ± 2.11% of Chi and 79.20 ± 5.63% of sHA no longer present. After 6 month, almost all of Chi and sHA were cleared from the body (Supplementary Fig. 7a). 99.67 ± 0.37% of Chi and 97.24 ± 1.11% of sHA were removed (Supplementary Fig. 7b).

We further demonstrated the functionality of sHAChiF by comparing its therapeutic effects using another post-surgical adhesion model: rat cecal abrasion, which is known to exhibit more severe post-surgical adhesions than the ischemic button model[5]. Post-surgical adhesions were induced by abrading the cecum and abdominal wall of

https://doi.org/10.1038/s41467-024-52753-0

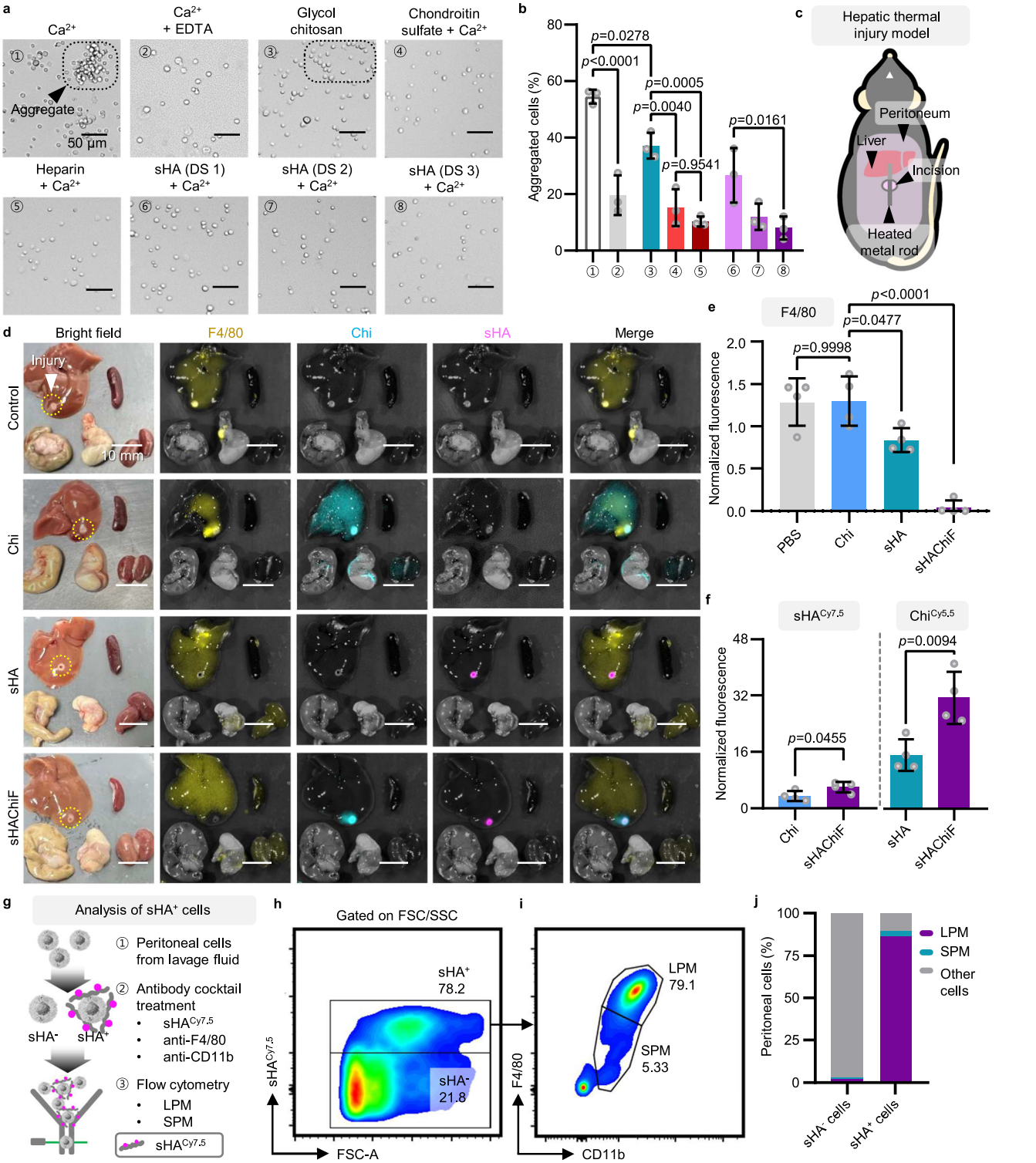

Fig. 5 | Disturbance of peritoneal macrophage aggregation by sHA in sHAChiF. **a** Representative images of the aggregation behavior of rat peritoneal macrophages following treatment with various polysaccharides (Scale bar = 50 μm). **b** Quantification of aggregated rat peritoneal macrophages treated with various polysaccharides. **c** Schematic illustration of the mouse hepatic thermal injury model. **d** Representative images of mouse organs in the mouse hepatic thermal injury model after treatment with sHAChiF, showing F4/80 (yellow; pseudocolor), Chi (cyan; pseudocolor), and sHA (magenta; pseudocolor) (Scale bar = 10 mm). **e** Quantification of F4/80 expression on the wound by measuring fluorescence with APC/Fire™ anti-F4/80 antibody, normalized by fluorescence levels in the normal liver. **f** Quantification fluorescence of sHA from $sHA^{Cy7.5}$ on the wound (left) and Chi from $Chi^{Cy5.5}$ on the wound (right), normalized by fluorescence from normal liver. **g** Schematic illustration of analysis for sHA uptake behavior of peritoneal cells using flow cytometry. Peritoneal cells gated based on sHA^+ population (**h**), grouping of sHA^+ LPM and sHA^+ SPM by F4/80 and CD11b expression levels (**i**), the ratio of peritoneal cell populations distinguishing between sHA^- and sHA^+ populations (**j**). Data are shown as mean ± SD ($n = 3$) independent samples in **a**,**b**; $n = 4$ independent samples in **d**–**f**; $n = 4$ independent samples in **h**–**j**. Two-tailed unpaired t-test was used for statistical analysis of **f**. One-way ANOVA with Tukey post-hoc test was used for statistical analysis of **b**,**e**. Source data are provided as a Source Data file. Image was created using PowerPoint.

rats, and sHAChiF was applied to the abraded sites (Supplementary Fig. 8a). The rats were sacrificed at 7 d post-surgery and the severity of adhesions was assessed. PBS and Seprafilm® treatments served as negative and positive controls, respectively. Similar to the ischemic button model, sHAChiF significantly reduced adhesion formation, recording 0 % adhesion formation (Supplementary Fig. 8b,\c). Masson's trichrome staining demonstrated that the control and Seprafilm® groups resulted in tight adhesion between the cecum and the abdominal wall (Supplementary Fig. 8d). However, in the sHAChiF-treated groups, the cecum and abdominal wall tissues were clearly separated. The collagen thickness of the tissues in the sHAChiF group was 4.5-fold, and 3.1-fold lower than in the control and Seprafilm® groups, respectively (Supplementary Fig. 8e).

Immunomodulatory function of sHAChiF hydrogel treated in the rat post-surgical adhesion model

The incomplete protection offered by Seprafilm® against post-surgical adhesion suggested that relying solely on a physical barrier between injured tissues was insufficient. To assess the potential of sHAChiF in exerting an anti-inflammation effect, we conducted IVIS imaging of inflammation in a mouse ischemic button model (Supplementary Fig. 9a). For this purpose, we used ProSense® 750Fast, a commercially available NIR fluorescent dye that became active in the presence of cathepsin in inflammation areas[38]. In the experimental setup, sHAChiF was applied to half of the ischemic buttons, resulting in a significant reduction in the fluorescence of ProSense® 750Fast (Supplementary Fig. 9b). The application of sHAChiF led to a remarkable decrease in inflammatory fluorescence, with levels dropping to 44.81 ± 19.20% compared to the control (Supplementary Fig. 9c). To elucidate which factors enhanced the performance of sHAChiF as an adhesion barrier, we isolated tissue samples from the ischemic button model 7 d after surgery and analyzed their inflammation levels.

Immunohistochemical analysis targeting iNOS and Arg1 in the ischemic buttons revealed that $iNOS^+$ M1 macrophages were primarily recruited to the buttons of peritoneal adhesion in the control and Seprafilm® groups (Fig. 6i). On the other hand, the sHAChiF groups exhibited a higher presence of $Arg1^+$ M2 macrophages. The M1/M2 ratio demonstrated a significant difference between the groups (Fig. 6j). The M1/M2 ratio in the control group was 4.46 ± 1.40, and in the Seprafilm® group, it was 4.28 ± 1.11. By comparison, the sHAChiF group's ratio was 0.08 ± 0.08. In summary, sHAChiF played a pivotal role in modulating M1-M2 macrophage polarization, leading to an increase in M2 macrophages within the ischemic button.

Furthermore, sHAChiF exhibited a notable reduction in the levels of pro-inflammatory cytokines in the ischemic button model (Fig. 6k–m). 4 d after surgery, blood samples were collected from the rat jugular vein, and serum samples were isolated for cytokine analysis. We didn't use peritoneal lavage fluid for cytokine analysis because the cytokines in the peritoneal fluid could be cleared rapidly[39]. The pro-inflammatory cytokines were effectively diminished in the sHAChiF group. IL−1β levels were 3.7-fold (Fig. 6k), IL-6 levels were 2.7-fold lower (Fig. 6l), and TNF-α levels were 2.9-fold lower (Fig. 6m) compared to the control groups. In contrast, Seprafilm® did not demonstrate superior results to the control group in the cytokine analysis, except for IL-6 expression, which exhibited a slight decrease compared to the control group (Fig. 6l). The trend of attenuated pro-inflammatory cytokines in the sHAChiF group was also observed in the sample taken 7d post-surgery (Supplementary Fig. 10). The values for IL-1β (Supplementary Fig. 10a), IL-6 (Supplementary Fig. 10b), and TNF-α (Supplementary Fig. 10c) were 1.5-fold, 2.3-fold, and 2.2-fold lower than the control group. That is, the sHAChiF effectively prevented peritoneal adhesion following surgery by attenuating pro-inflammatory cytokines through the M2 polarization of peritoneal macrophages at the ischemic buttons.

Discussion

To prevent post-surgical adhesions, applying adhesion barriers to the surgical trauma is a primary strategy. However, commercial adhesion barriers face limitations that hinder their effective use. Issues such as an inefficient delivery system, handling difficulties, and inflammation after surgery undermine their efficacy.

Utilizing sHA presents a promising solution for next-generation adhesion barriers. sHA possesses several properties beneficial for biomaterial applications. Its anti-inflammatory function can modulate the immune response by transforming peritoneal macrophages into M2 phenotype. Additionally, the anionic charge of sHA can repel peritoneal macrophages and inhibit aggregation, a key step in post-surgical adhesion formation. Moreover, sHA's resistance to degradation enables the adhesion barrier to remain effective for extended periods, exceeding 14 d.

We harnessed the advantages of sHA by incorporating it into a hydrogel. Blending sHA with Chi facilitated rapid gelation through polyelectrolyte complex formation. Sprayability was also possible. Our customized dual sprayer delivery system enabled sHAChiF gel to be applied over a wide area rapidly. Another advantage of the customized-dual sprayer is convenience to use. Inconvenience and complex conditions to use were main causes of low usage of conventional adhesion barriers during surgeries. Only by pressing a switch, the sHA/F127 and Chi/F127 solutions were sprayed simultaneously. The sHA/F127 and Chi/F127 droplets were blended during spraying, resulting in dramatic increase of viscosity of the mixture and gelation. This physical barrier effectively separates the injured peritoneum, overcoming the limitations of conventional adhesion barriers.

Furthermore, the sHAChiF hydrogel demonstrated unique actions on peritoneal macrophages: (1) Anti-inflammation and (2) Agreggation prevention. First, the anti-inflammation. The sHA polarized macrophages towards the anti-inflammatory M2 phenotype, thereby reducing pro-inflammatory cytokine expression. This mitigated the inflammatory environment associated with peritoneal injury, decreasing adhesion mechanism activation. Second, the aggregation prevention. the anionic charge of sHA interacted with scavenger receptors expressed on LPMs and this hindered the aggregation of peritoneal macrophages on the surgical trauma site. The LPM aggregation is known as the initiation step of post-surgical adhesion. By repelling these macrophages, the sHAChiF hydrogel weakened the formation of post-surgical adhesions. The combination of these properties with physical barrier formation effectively blocked adhesion formation in a murine ischemic button model.

In summary, we have developed a sprayable sHAChiF hydrogel that undergoes in situ gelation through the blending of sHA/F127 and Chi/F127 components using a dual-sprayer system. This spray system ensured uniform dispersion onto the target area, enhancing efficiency, convenience, and time-saving benefits. Notably, sHA played a pivotal role in the functionality of the sHAChiF hydrogel by establishing a structural framework via polyelectrolyte complex formation with Chi. The stabilization provided by pluronic® F127, contribute to stabilize the polyelectrolyte complex and established an additional network by thermogelation. Furthermore, sHA played a crucial role in mitigating inflammation and promoting M2 polarization in peritoneal macrophages, enhancing the hydrogel's efficacy in a rat post-surgical model. Consequently, this sprayable sHAChiF hydrogel demonstrated significant potential for clinical applications as an adhesion barrier.

Methods

Ethical statement

All animal experiments were approved by the Institutional Animal Care & Use Committee of Seoul National University (Approval number: SNU-230329-1 and SNU-230607-4). All mice were housed at 12-h light-dark cycle within 21-25 °C and 40-60 % humidity.

https://doi.org/10.1038/s41467-024-52753-0

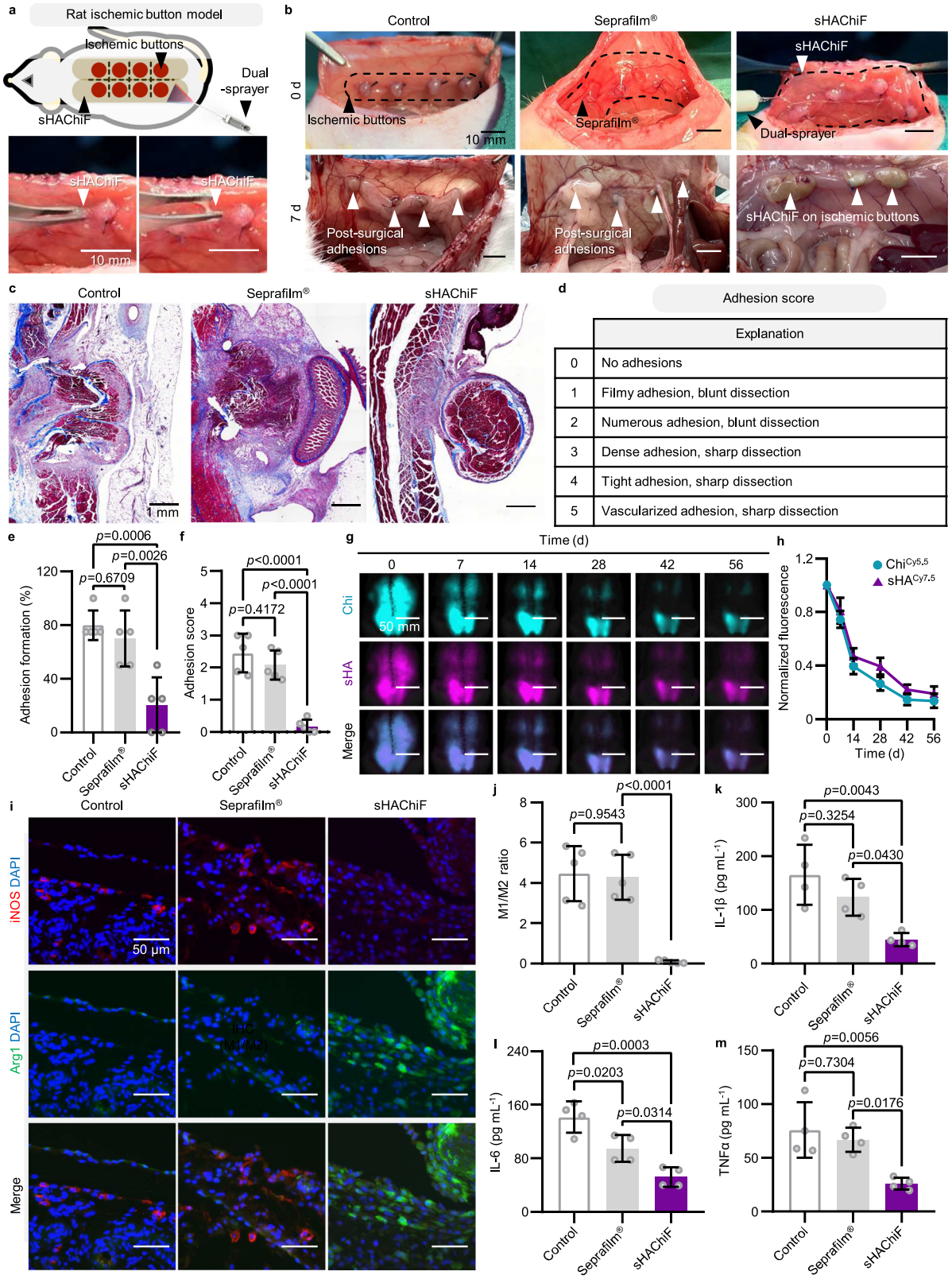

Materials

Dowex® 50 W X8 (Catalog # 44509), Tetrabutylammonium hydroxide 30-hydrate (TBA; Catalog # 86859), Sulfur trioxide *N*,*N*-dimethylformamide complex (SO_3-DMF; Catalog # 373680), Sodium hydroxide (NaOH; Catalog # S8045), Chitosan (Chi, 75 % deacetylation, Mw ≈ 50 ~ 190 kDa; Catalog # 448869), Pluronic® F127 (Catalog # P2443), Lipopolysaccharide from *Escherichia coli* O111:B4 (LPS; Catalog # L4391), Latex bead (Polystyrene; Catalog # LB30), Luminol sodium salt (Catalog # A4685), Calcium chloride (Catalog # 442909), and *N*-hydroxysuccinimide (NHS; Catalog # 130672) were purchased from Sigma Aldrich (USA). Hyaluronic acid (HA, Mw 1.01 MDa ~ 1.8 Mda; Catalog # HA15M) was purchased from Lifecore Biomedical (USA). *N*-(3-dimethyl aminopropyl)-*N*′-ethyl carbodiimide (EDC; Catalog # 22981), Calcein AM (Catalog # C3099), and Ethidium homodimer

Fig. 6 | Prevention of peritoneal adhesion in rat ischemic button model using sHAChiF. a Schematic illustrations of modeling rat ischemic button model with sHAChiF (top) and representative images of sHAChiF treated on the ischemic buttons (Scale bar = 10 mm). **b** Representative images of rat ischemic button model on d 0 and d 7 after surgery (Scale bar = 10 mm). **c** Representative Masson's trichrome staining images of adhesive tissues on d 7 after surgery (Scale bar = 1 mm). **d** Specification of scoring severity of peritoneal adhesion. **e** Adhesion formation rates with adhesion scores of sHAChiF per rat. **f** Quantification of the adhesion scores of dual-sprayable hydrogels. **g** Representative IVIS images of fluorescence by $Chi^{Cy5.5}$ (cyan; pseudocolor) and $sHA^{Cy7.5}$ (magenta; pseudocolor) in dual-sprayable hydrogels at various time points (Scale bar = 50 mm). **h** In vivo retention profiles of $Chi^{Cy5.5}$ and $sHA^{Cy7.5}$ in dual-sprayable hydrogels over time through calculation of fluorescence intensity, normalized by fluorescence at d 0. **i** Representative iNOS and Arg1 immunofluorescence staining images of adhesive tissues on d 7 after surgery (Scale bar = 50 μm). **j** Quantification of M1/M2 ratio of peritoneal macrophages in adhesive tissues on d 7 after surgery. Quantification of pro-inflammatory cytokines IL−1β (**k**), IL-6 (**l**), and TNF-α (**m**) from rat serum on d 4 after surgery. Data are shown as mean ± SD ($n = 5$ independent samples in **b**–**f**; $n = 4$ independent samples in **g**,**h**; $n = 5$ independent samples in **i**, **j**; $n = 4$ independent samples in **k**–**m**). One-way ANOVA with Tukey post-hoc test was used for statistical analysis of **e**,**f**,**j**–**m**. Source data are provided as a Source Data file. Image was created using PowerPoint.

(Catalog # E1169) were purchased from Thermo Fisher Scientific (USA). Hydrochloric acid (HCl; Catalog # 0009-08012), and *N*,*N*-Dimethylformamide (Catalog # 30574105) were purchased from DaeJung (Korea). AIN-93G purified rodent diet (Catalog # TD.94045) was purchased from Envigo (USA). Isoflurane (Catalog # 657801261) was purchased from Hana Pharm (Korea). Seprafilm® (Catalog # 664103) was purchased from Baxter Healthcare SA (Switzerland). ELISA MAX™ Mouse TNF-α ELISA kit (Catalog # 430904), and LEGENDplex™ rat inflammation panel (Catalog # 741395) were purchased from BioLegend (USA). Cyanine5.5 (Cy5.5) NHS ester (Catalog # 27020) and Cyanine7 (Cy7) amine (Catalog # 260C0) were purchased from Lumiprobe (USA). ProSense® 750Fast (Catalog # NEV11171) was purchased from Perkin Elmer (USA). Detailed information of antibodies was provided in Supplementary Table 1.

Fabrication of HA-TBA

HA-TBA was synthesized in accordance with established protocols[40]. Initially, HA (2 g) was dissolved in deionized water (200 mL). Subsequently, Dowex® 50 W X8 (20 g) was incorporated to the HA solution, and the mixture was stirred overnight. Following the removal of Dowex® 50 W X8 through filtration, TBA was slowly added until the solution reached pH 9. The resulting solution was then frozen, lyophilized, and stored for further use.

Fabrication of sHA

sHA was synthesized from HA-TBA as previously reported[41]. HA-TBA (500 mg) was dissolved in anhydrous DMF (100 mL) under N_2 purging for 3 h. Once dissolution was completed, SO_3-DMF (3 g) was added to the solution and reacted for 1 h. The pH of the solution was adjusted to 9 by the addition of NaOH (1 M) for product purification. Subsequently, cold ethanol was added to precipitate the product, and the obtained precipitate was filtered and washed with deionized water three times. The resulting product was then dissolved in deionized water, and the solution was dialyzed for 3 d with water changes twice a day. The final product was frozen, lyophilized, and stored for further use. The degree of substitution of sulfonic acid groups (DS) per uronic acid was determined with an estimation of the ratio between sulfur content and carbon content using an elemental analyzer (TruSpec® Micro CHNS, LECO, USA), and the molecular weights were analyzed by gel permeation chromatography (GPC, Ultimate 3000, Dionex, USA). Reaction conditions and degree of sulfation are shown in Supplementary Table 2.

Synthesis of NIR dye-conjugated sHA and Chi

Fluorophore conjugation to sHA and Chi was carried out with slight modifications to previous procedures[42]. Briefly, sHA (560 mg, 1 mmol) was dissolved in a DMSO solution (100 mL, DMSO:deinonized water = 1:1). Once sHA was fully dissolved, EDC (191.7 mg, 1 mmol) was added to the solution and stirred at 300 rpm for 15 min at room temperature. The pH was adjusted to 7 with NaOH (1 M) and NHS (115.1 mg, 1 mmol) was added to the solution, left to react for 15 min. Subsequently, Cy7.5-amine (8.2 mg, 0.01 mmol) was added to the solution and the reaction took place for 48 h in the dark. The final product was dialyzed with water changes every 6 h for 3 d, collected and lyophilized. Chi was conjugated with Cy5.5-NHS in a similar process. Chi (365 mg, 1 mmol) was dissolved a DMSO solution (100 mL, DMSO:deinonized water = 1:1), and Cy5.5-NHS (7.7 mg, 0.01 mmol) was added to the solution. The reaction occurred in the dark for 48 h, followed by dialyzed and lyophilization.

Preparation of sHAChiF

Pluronic® F127 solution (19 or 20%) was prepared in PBS. Then, separate solutions of sHA (2 %) and Chi (2 %) were prepared within the Pluronic® F127 (19 or 20%) solution, denoted as sHA/F127 and Chi/F127, respectively. Because of the insolubility of Chi in neutral pH, the Chi was solubilized by Pluronic® F127 (19 or 20%) in HCl solution or acetic acid (0.1 M) first and the pH was adjusted to be 7.0 by Pluronic® F127 (19 or 20%) in PBS. Subsequently, the sHAChiF hydrogel was produced by mixing sHA/F127 and Chi/F127 using various formulations.

Gelation conditions of sHAChiF

In order to determine the optimal conditions for gelation, various formulations of sHA/F127 and Chi/F127 were investigated. Initially, inverted vial tests using the Pluronic® F127 (19%) were conducted. sHA/F127 and Chi/F127 solutions with different sHA and Chi concentration (1.2, 1.4, 1.6, 1.8, and 2.0%) were prepared within the F127 (19%) solution. For each combination, equal volumes of sHA/F127 and Chi/F127 solutions were mixed in a glass vial placed on ice, resulting in the creation of 25 sHAChiF combinations. These solution mixtures were incubated on ice for 30 min, then brought to room temperature for 1 h, followed by vial inversion, and left at room temperature for an additional 15 min to stabilize the gel condition. This entire procedure was repeated using the Pluronic® F127 (20%) solution.

Evaluation of spray conditions of Chi/F127 solution

Due to its viscous characteristics, the viscosity of the Chi/F127 solution was optimized by screening the concentration of Chi. Viscosity measurements of the Chi/F127 solutions were measured through rheological analysis employing a rheometer (ARES, Rheometric Scientific, UK). The Chi/F127 solutions with varing concentrations were dispensed onto the base plate (25 mm in diameter) of the rheometer. Subsequently, the Chi/F127 solutions (300 μL) were sandwitched by a flat probe (25 mm in diameter). The gap size was 0.6 mm. The viscosities (Pa s) of the loaded samples were assessed over a range of shear rates, spanning from 10 ~ 1000 s^{-1}.

Mechanical characterization of sHAChiF

The elastic moduli of the sHAChiF were measured by a rheometer (ARES, Rheometric Scientific, UK). The sHAChiF were loaded to the base plate (25 mm in diameter) of a rheometer and the gels (300 μL) were sandwitched by a flat probe (25 mm in diameter). The gap size was 0.6 mm. The amplitude sweep test was implemented with 0.1 ~ 100 % shear strain at a constant frequency (10 rad s^{-1}). The elastic modulus (G′) at the linear viscoelastic region was quantified. The frequency sweep

test was performed with 0.1 ~ 100 rad s^{-1} at a constant shear strain (5%). 3-intervals thixotropy tests were conducted, with a shear rate of 10 s^{-1} in interval 2. The duration of each time interval was 90, 20, and 90, respectively. Rheological tests were repeated at both 25 °C and 37 °C.

Sprayability of sHAChiF

sHA/F127 and Chi/F127 solutions with the inclusion of inks (Pluronic® F127 only: Black, sHA/F127: Red, Chi/F127: Blue) were prepared. These solutions were then loaded onto a dual-sprayer and sprayed onto paper, maintaining a distance of 5 cm from the nozzle. A comprehensive description of the test conditions can be found in Supplementary Table 3. The resulting spray-covered papers were allowed to air-dry overnight. Subsequently, they were collected, scanned, and the distribution of droplets was analyzed using a method previously reported, employing ImageJ[43]. The scanned spray pattern was cropped to a 1000 by 1000 pixel box. The X and Y coordinates of the droplets were recorded and adjusted to center the spray pattern. Coverage was determined as a percentage of the whole image.

In vitro cytocompatibility of sHAChiF

The murine fibroblast cell line NIH-3T3 was obtained from ATCC (Catalog no. CRL-1658). NIH-3T3 cells (3×10^4 cells per well) were seeded in 48-well plates and incubated in DMEM containing FBS (10%) under 37 °C, 5% CO_2. After incubation for 24 h, cells were washed with warm PBS, and fresh DMEM with sHA (0.1%), Chi (0.1%), and sHAChiF (0.1%) were added to respective groups. Cells were incubated with the materials for 24 h, stained with Calcein AM (2000:1 dilution by PBS) and Ethidium homodimer (500:1 dilution by PBS) and visualized with EVOS™ FL Auto 2 (Thermo Fisher, USA).

In vitro immunomodulation characteristics by sHAChiF

The murine macrophage cell line RAW264.7 was obtained from ATCC (Catalog no. TIB-71). RAW264.7 cells (1×10^5 cells per well) were seeded on coverslips in 6-well plates and incubated with RPMI media supplemented with FBS (10%). Cells were incubated for 18 h, and the following day, the media was replaced with new RPMI media containing sHA, Chi (0.1%), or sHAChiF (0.1%). After an additional 24 h of incubation, LPS (100 ng mL^{-1}) was treated to all wells and cells were incubated for another 24 h. The supernatants were collected, centrifuged at 1977 g, aliquoted, and frozen. Cells on coverslips were fixed, washed, blocked with goat serum, and treated with anti-CD206 and anti-iNOS antibodies (200:1 dilution). Secondary antibodies Alexa Fluor™ 488 goat anti-rabbit IgG and Alexa Fluor™ 594 goat anti-mouse IgG (500:1 dilution) were used to label the primary antibodies. After a final wash, coverslips were mounted with DAPI-containing mounting medium. The slides were imaged using EVOS™ FL Auto 2 (Thermo Fisher, USA). The TNF-α level of the supernatant was quantified by ELISA MAX™ Mouse TNF-α ELISA kit following the manufacturer's instructions.

In vivo biocompatibility of sHAChiF

In vivo biocompatibility assessment of sHAChiF was conducted through subcutaneous luminol activity measurement, following established methods[44,45]. Female C57BL/6 mice, aged 8 wks (Nara Biotech, Korea), were utilized for this study. The mice were divided into six experimental groups: (1) Negative control with PBS, (2) Positive control with polystyrene latex beads (3) Pluronic F127® only, (4) Chi/F127, (5) sHA/F127, and (6) sHAChiF. Dorsal skin hair on the mice was removed using a hair clipper. Subsequently, each sample (50 µL) was subcutaneously injected into the dorsal skin of the mice, resulting in six implantation sites per mouse. The mice were maintained on an AIN-93G purified rodent diet to minimize background fluorescence interference. After 4 d, each mouse received a peritoneal injection of luminol sodium salt (200 mg kg^{-1}). Following a 15-min interval, luminol activity at the implantation sites was measured using IVIS Spectrum (PerkinElmer Inc., USA). Throughout the procedure, mice were anesthetized with isoflurane inhalation. Signal intensities from the images were quantified using Living Image® software, with a 5 mm diameter region of interest (ROI) for luminescence measurement, and each signal was normalized against the background signal obtained from a normal skin area.

In vivo retention study of sHAChiF in mice

The in vivo retention of sHAChiF was evaluated by implanting $sHA^{Cy7.5}$/F127, $Chi^{Cy5.5}$/F127, and sHAChiF with $sHA^{Cy7.5}$/$Chi^{Cy5.5}$ into BALBc/Nu mice, aged 8 wk (Nara Biotech, Korea). Each material (50 µL) was loaded into a 1 mL-syringe and injected subcutaneously into the middle of the back of each mouse. The degradation of each group was assessed by quantification of the fluorescence signals imaged by the IVIS system.

In vitro peritoneal macrophage aggregation test

The peritoneal macrophage aggregation test was adapted from macrophage aggregometry tests previously described[23]. Peritoneal lavage fluid was extracted to isolate the peritoneal macrophages, by injecting ice-cold EDTA (2 mM, in PBS) into the rat peritoneum, and recollecting the fluid with a 5 mL-syringe. The lavage fluid was centrifuged at 494 g for 8 min, and the cells were cultured on a petri dish for 4 h using RPMI media supplemented with FBS (15%). The adherent cells were collected, washed, and dispersed in Ca^{2+} solution (2 mM, 100 µL) or DPBS solution. An agonist solution comprised of either chondroitin sulfate, glycol chitosan, heparin, or sHA (DS: 1, 2, and 3) dissolved in either DPBS or Ca^{2+} solution was prepared at a concentration of 2 mg mL^{-1}. Agonist solution (185 µL) and cell suspension (15 µL) was mixed in a 1 mL-glass vial and placed on an orbital shaker. Incubated solution (50 µL) were collected from each vial at a time period of 0, 5, 10, and 15 min, placed in a 96-well, and observed by light microscopy.

In vivo imaging of sHAChiF effect on peritoneal macrophages

Prior to the experiment, APC/Fire™ anti-F4/80 antibodies (50:1 dilution, 100 µL) were injected in C57BL/6 mice. Following antibody administration, a thermal injury model was induced in the mice, adapted from a sterile inflammation induction method[46]. In brief, a midline skin incision was made in the C57BL/6 mice, and a hole (3 mm) was induced on the peritoneum to expose the liver. A pre-heated metal rod was applied to the liver for 3 s to create a sterile thermal wound. Immediately, samples ($sHA^{Cy7.5}$/F127, $Chi^{Cy5.5}$/F127, and sHAChiF with $sHA^{Cy7.5}$/$Chi^{Cy5.5}$) were randomly distributed within the peritoneal cavity of each group of mice. The peritoneal walls were sutured, and the mice were placed in prone position for 20 min. After 20 min, mice were sacrificed, and their organs (liver, spleen, cecum, stomach, kidneys) were harvested, washed, and imaged using the IVIS Spectrum. The spectral unmixing technique was used to separate the fluorescent signals.

Flow cytometry of peritoneal lavage fluid

Antibody cocktail for flow cytometry was prepared before experiment: $sHA^{Cy7.5}$ (0.001%), Pacific Blue™ anti-F4/80 antibody (50:1 dilution), and Alexa 488™ anti-CD11b antibody (50:1 dilution). C57BL/6 mice were euthanized and EDTA solution (1 mM, 5 mL, in PBS) was injected to peritoneum. The lavage fluid was recollected, centrifuged at 266 g for 5 min. After supernatant removal, the antibody cocktail (100 µL) was treated to the peritoneal cells for 20 min. The cells were washed and flow cytometry was implemented. Singlet cells were gated by FSC/SSC first. The cells were further gated, base on surface marker expressions. LPM population was gated as $CD11b^{high}$ $F4/80^{high}$, and SPM population was gated as $CD11b^{int}$ and $F4/80^{int}$. Each LPM and SPM population was additionally gated by $sHA^{Cy7.5}$.

Application of sHAChiF in mouse post-surgical adehsion model

Female C57BL/6 mice aged 8 wks (Nara Biotech, Korea) were used to generate the ischemic button model. The injury was induced as previously described[23]. In preparation for surgery, mice were anesthetized through inhalation of isoflurane one day prior to the procedure. The

ventral skin of the mice was depilated using a hair clipper, and depilatory cream was applied. To prevent potential skin inflammation caused by any residual depilatory cream, the depilated areas were gently cleansed. Immediately before the surgery, mice were anesthetized following the same procedure as described earlier. Presterilization of the ventral skin of the mice was achieved by applying Povidone-Iodine and ethanol (70 %). Surgical access was gained by making an incision along the midline of the mice abdomen, thereby exposing the peritoneal cavity. A small section of the peritoneal wall was gripped, and a 6-0 nylon suture was pierced through the middle of the grasped section. A knot was formed, and the suture was lassoed around the grasped tissue and knotted again to form a button. 2 buttons were made on each wall, totaling to 4 buttons on each mice. Immediately after button formation, sHAChiF was administered on the half of the buttons. The midline was closed by suture, and the mice were maintained on an AIN-93G purified rodent diet to minimize background fluorescence interference. 1 d before imaging, ProSense® 750Fast was injected to the mice through tail vein. The mice in supine position were imaged by IVIS 1 wk after surgery.

Application of sHAChiF in rat post-surgical adehsion model

Female Spraque-Dawley (SD) rats weighing 200 ~ 250 g (Daehan Bio-Link Co., Korea) were used to generate the ischemic button model and cecal abrasion medel. In the rat ischemic button model, the injury was induced by similar process as described above. Before the surgery, rats were anesthetized with isoflurane, and their ventral skin was prepared by depilation and cleaning to prevent potential skin inflammation from residual depilatory cream. On the day of surgery, the rats were anesthetized again and their ventral skin was sterilized with Povidone-Iodine and ethanol (70 %). The peritoneal cavity was exposed by a midline incision in the rat's abdomen. The suture was knotted to form a button by a 4-0 nylon suture. 4 buttons were created on each peritoneal wall, resulting in a total of 8 buttons per rat. Immediately after button formation, sHAChiF was applied to the buttons. Seprafilm® was used as a positive control. The midline incision was sutured closed, and the rats were sacrificed for analysis 1 wk after the surgery. The severity of adhesions was assessed by opening the peritoneum and employing the Launder score.

In the rat ecal abrasion model, the surface of the cecum was consistently abraded with sandpaper until petechial hemorrhage occurred (Area = 2.5 cm*1 cm). Additionally, the abdominal wall was scraped using a scalpel to create a matching area (Area = 2.5 cm*1 cm). Following the abrasions, sHAChiF was applied to both abraded sites. PBS and Seprafilm® were used as negative and positive controls, respectively. To prevent peristaltic movement of the intestine, the abraded area of the cecum and abdominal wall was securely fixed with 4-0 nylon sutures. The rats were sacrificed for analysis 1 wk after the surgery.

In vivo retention of sHAChiF in rat post-surgical adehsion model

The degradation profile of sHAChiF in the peritoneal cavity was assessed in a rat ischemic button model. Buttons were formed on SD rats as described above. sHAChiF with $sHA^{Cy7.5}$/$Chi^{Cy5.5}$ (500 µL per each peritoneal wall) were sprayed inside the peritoneum to thoroughly cover the formed buttons. After surgery, the fluorescent signals were monitored using the IVIS system. To separate the fluorescence from $sHA^{Cy7.5}$ and $Chi^{Cy5.5}$, each Cy5.5 and Cy7.5 was measured for calibration. After calibration, each fluorescence from the $sHA^{Cy7.5}$ and $Chi^{Cy5.5}$ were analyzed through spectral unmixing.

Histological analysis of rat post-surgical adhesion model

About 7 d post-surgery, the rats were euthanized by exposure to excessive CO_2 gas. Subsequently, laparotomy was performed, and the extent of adhesion in each group was visually documented and assessed based on the adhesion score criteria, as detailed in Fig. 5d. Tissue samples were then procured, fixed in paraformaldehyde (4%), and subsequently embedded in paraffin. The paraffin-embedded tissue sections were subjected to histological examination through Masson's trichrome staining and immunohistochemical analysis. In immunohistochemistry, the tissue sections were prepared, boiled in Tris-EDTA buffer (50 mL, pH 9.0) for antigen retrieval, and permeabilized. The samples were blocked with goat serum, and treated with anti-iNOS and anti-Arg1 antibodies (200:1 dilution). Secondary antibodies Alexa Fluor™ 488 goat anti-rabbit IgG and Alexa Fluor™ 594 goat anti-mouse IgG (500:1 dilution) were used to label the primary antibodies. DAPI-containing mounting solution was used to mount the samples, and samples were imaged with the EVOS™ FL Auto 2 (Thermo Fisher, USA).

Quantification of rat cytokine level

About 4 d post-surgery, blood samples were obtained from all groups of rats via the jugular vein. Within 30 min after collection, the blood samples underwent centrifugation for 10 min at 1000 g to remove clots. The resulting supernatant serums were isolated and employed for the analysis of the serum cytokine profile. The concentration of inflammatory cytokines, including IL-1β, IL-6, and TNF-α, in rat serum was quantified utilizing a LEGENDplex™ rat inflammation panel in accordance with the manufacturer's protocol.

Statistics & reproduciblity

The data analysis was conducted in a blind fashion. Data were analyzed using GraphPad Prism 8. Results were presented as the mean ± standard deviation (SD), with replication in at least three independent experiments. Two-tailed unpaired t-test was used for comparisons between two groups. One-way ANOVA with Tukey post-hoc was used for multiple groups. The statistical significance was defined as $p < 0.05$.

Reporting summary

Further information on research design is available in the Nature Portfolio Reporting Summary linked to this article.

Data availability

All data supporting the findings of this study are available within the article and its supplementary information. Additional data can be provided by the corresponding author upon request. Source data are provided with this paper.

References

1. Huang, C. & Ding, D. C. Outcomes of adhesion barriers in gynecologic surgeries: a retrospective study at a medical center. *Medicine (Baltimore)* **98**, e18391 (2019).
2. Arung, W., Meurisse, M. & Detry, O. Pathophysiology and prevention of postoperative peritoneal adhesions. *World J. Gastroenterol.* **17**, 4545–4553 (2011).
3. Sikirica, V. et al. The inpatient burden of abdominal and gynecological adhesiolysis in the US. *BMC Surg* **11**, 13 (2011).
4. Okabayashi, K. et al. Adhesions after abdominal surgery: a systematic review of the incidence, distribution and severity. *Surg. Today* **44**, 405–420 (2014).
5. Tang, J. Y., Xiang, Z. Y., Bernards, M. T. & Chen, S. F. Peritoneal adhesions: Occurrence, prevention and experimental models. *Acta Biomater* **116**, 84–104 (2020).
6. Postoperative adhesions in gynecologic surgery: a committee opinion. *Fertil. Steril.* **112**, 458-463 (2019).
7. Lauder, C. I., Garcea, G., Strickland, A. & Maddern, G. J. Abdominal adhesion prevention: still a sticky subject? *Dig. Surg.* **27**, 347–358 (2010).
8. Hackethal, A. et al. Awareness and perception of intra-abdominal adhesions and related consequences: survey of gynaecologists in German hospitals. *Eur. J. Obstet. Gynecol. Reprod. Biol.* **150**, 180–189 (2010).

9. Okubo, S., Shindoh, J., Kobayashi, Y. & Hashimoto, M. Safety of a new spray-type adhesion barrier (AdSpray®) in liver surgery. *J. Hepatobiliary Pancreat. Sci.* **27**, 648–654 (2020).
10. Wiseman, D. M., Gottlick-Iarkowski, L. & Kamp, L. Effect of different barriers of oxidized regenerated cellulose (ORC) on cecal and sidewall adhesions in the presence and absence of bleeding. *J. Invest. Surg.* **12**, 141–146 (1999).
11. Becker, J. M. et al. Prevention of postoperative abdominal adhesions by a sodium hyaluronate-based bioresorbable membrane: a prospective, randomized, double-blind multicenter study. *J. Am. Coll. Surg.* **183**, 297–306 (1996).
12. Konar, S. et al. Silk fibroin hydrogel as physical barrier for prevention of post hernia adhesion. *Hernia* **21**, 125–137 (2017).
13. Ward, B. C. & Panitch, A. Abdominal adhesions: current and novel therapies. *J. Surg. Res.* **165**, 91–111 (2011).
14. Helmecke, T. et al. Inflammation-Controlled Anti-Inflammatory Hydrogels. *Adv. Sci.* **10**, 2206412 (2023).
15. Hassanabad, A. F. et al. Prevention of post-operative adhesions: a comprehensive review of present and emerging strategies. *Biomolecules* **11** (2021).
16. Li, Z., Liu, L. & Chen, Y. Dual dynamically crosslinked thermosensitive hydrogel with self-fixing as a postoperative anti-adhesion barrier. *Acta Biomater* **110**, 119–128 (2020).
17. du Toit, L. C., Choonara, Y. E. & Pillay, V. An injectable nano-enabled thermogel to attain controlled delivery of p11 peptide for the potential treatment of ocular angiogenic disorders of the posterior segment. *Pharmaceutics* **13** (2021).
18. Kushan, E. & Senses, E. Thermoresponsive and injectable composite hydrogels of cellulose nanocrystals and pluronic F127. *ACS Appl. Bio. Mater.* **4**, 3507–3517 (2021).
19. Secer, S. & Tuncaboylu, D. C. Supramolecular poloxamer-based in situ gels with hyaluronic acid and cyclodextrins. *Int. J. Polym. Mater. Po.* **71**, 647–655 (2022).
20. Kulkarni, A. D. et al. Polyelectrolyte complexes: mechanisms, critical experimental aspects, and applications. *Artif. Cells Nanomed. Biotechnol.* **44**, 1615–1625 (2016).
21. Jouy, F. et al. Sulfated hyaluronan attenuates inflammatory signaling pathways in macrophages involving induction of antioxidants. *Proteomics* **17**, e1700082 (2017).
22. Hauck, S. et al. Collagen/hyaluronan based hydrogels releasing sulfated hyaluronan improve dermal wound healing in diabetic mice via reducing inflammatory macrophage activity. *Bioact. Mater.* **6**, 4342–4359 (2021).
23. Zindel, J. et al. Primordial GATA6 macrophages function as extravascular platelets in sterile injury. *Science* **371** (2021).
24. Chen, R. H., Lin, W. C. & Lin, J. H. Effects of Ph, Ionic-Strength, and Type of Anion on the Rheological Properties of Chitosan Solutions. *Acta Polym* **45**, 41–46 (1994).
25. Martínez, A., Chornet, E. & Rodrigue, D. Steady-shear rheology of concentrated chitosan solutions. *J. Texture Stud.* **35**, 53–74 (2004).
26. Feng, Q. et al. Sulfated hyaluronic acid hydrogels with retarded degradation and enhanced growth factor retention promote hMSC chondrogenesis and articular cartilage integrity with reduced hypertrophy. *Acta Biomater* **53**, 329–342 (2017).
27. Park, E. K. & Song, K.-W. Rheological evaluation of petroleum jelly as a base material in ointment and cream formulations: Steady shear flow behavior. *Arch. Pharmacal Res.* **33**, 141–150 (2010).
28. Hughes, B. & Saxena, A. K. Monitoring of body temperature during laparoscopic surgery following peritoneal insufflation with warm, humidified carbon dioxide using infrared camera. *J. Pediatr. Endosc. Surg.* **5**, 119–121 (2023).
29. Sumi, Y. et al. Simple and easy technique for the placement of seprafilm during laparoscopic surgery. *Indian J. Surg.* **77**, 1462–1465 (2015).
30. Kim, S. H. et al. Tissue adhesive, rapid forming, and sprayable ECM hydrogel via recombinant tyrosinase crosslinking. *Biomaterials* **178**, 401–412 (2018).
31. He, J. J., McCarthy, C. & Camci-Unal, G. Development of hydrogel-based sprayable wound dressings for second- and third-degree burns. *Adv. Biomed. Res.* **1**, 2100004 (2021).
32. Krielen, P. et al. Cost-effectiveness of the prevention of adhesions and adhesive small bowel obstruction after colorectal surgery with adhesion barriers: a modelling study. *World J. Emerg. Surg.* **14**, 41 (2019).
33. Stommel, M. W., Strik, C., ten, Broek, R. P. & van Goor, H. Efficacy and safety of the C-Qur™ Film Adhesion Barrier for the prevention of surgical adhesions (CLIPEUS Trial): study protocol for a randomized controlled trial. *Trials* **15**, 378 (2014).
34. Chandel, A. K. S., Shimizu, A., Hasegawa, K. & Ito, T. Advancement of biomaterial-based postoperative adhesion barriers. *Macromol. Biosci.* **21**, 2000395 (2021).
35. Tseng, J. C. & Kung, A. L. In vivo imaging of inflammatory phagocytes. *Chem. Biol.* **19**, 1199–1209 (2012).
36. Fujita, M. et al. Preventing post-surgical cardiac adhesions with a catechol-functionalized oxime hydrogel. *Nat. Commun.* **12**, 3764 (2021).
37. Comparison of thermal burn-induced and excisional-induced scarring in animal models: a review of the literature. *Adv. Wound Care*. **11**, 150-162 (2022).
38. Vegas, A. J. et al. Combinatorial hydrogel library enables identification of materials that mitigate the foreign body response in primates. *Nat. Biotechnol.* **34**, 345–352 (2016).
39. Chung, D. R. et al. CD4+ T cells regulate surgical and postinfectious adhesion formation. *J. Exp. Med.* **195**, 1471–1478 (2002).
40. Möller, S. et al. Synthesis and antiherpetic activity of carboxymethylated and sulfated hyaluronan derivatives. *Carbohyd. Polym.* **90**, 608–615 (2012).
41. Bhattacharya, D. S. et al. Sulfation modulates the targeting properties of hyaluronic acid to P-selectin and CD44. *ACS Biomater. Sci. Eng.* **6**, 3585–3598 (2020).
42. Choi, Y. et al. Deep tumor penetration of doxorubicin-loaded glycol chitosan nanoparticles using high-intensity focused ultrasound. *Pharmaceutics* **12** (2020).
43. Moakes, R. J. A., Davies, S. P., Stamataki, Z. & Grover, L. M. Formulation of a composite nasal spray enabling enhanced surface coverage and prophylaxis of SARS-COV-2. *Adv. Mater.* **33**, e2008304 (2021).
44. Bratlie, K. M. et al. Rapid biocompatibility analysis of materials via fluorescence imaging of mouse models. *Plos One* **5**, e10032 (2010).
45. Liu, W. E. et al. Real-time in vivo detection of biomaterial-induced reactive oxygen species. *Biomaterials* **32**, 1796–1801 (2011).
46. McDonald, B. et al. Intravascular danger signals guide neutrophils to sites of sterile inflammation. *Science* **330**, 362–366 (2010).

Acknowledgements

This work was financially supported by the Ministry of Science and ICT (NRF- 2021R1A2C2008821). The Institute of Engineering Research at Seoul National University provided research facilities for this work. This work also received financial support from the Korean Fund for Regenerative Medicine (KFRM) grant funded by the Korean government (21A0301L1-21).

Author contributions

W.S. and N.S.H. conceived and designed the experiments. W.S., C.L., H.J., and S.K. performed the experiments. W.S., and C.L. analyzed the data. W.S., C.L., and N.S.H. wrote and edited the manuscript. N.S.H. supervised the project. All authors revised and commented on the manuscript.

Competing interests
The authors declare no competing interests.

Additional information
Supplementary information The online version contains supplementary material available at https://doi.org/10.1038/s41467-024-52753-0.

Correspondence and requests for materials should be addressed to Nathaniel S. Hwang.

Peer review information *Nature Communications* thanks Guoxu Ma and the other, anonymous, reviewer(s) for their contribution to the peer review of this work. A peer review file is available.